Characterization of the morphology of cellular ceramics by 3D image processing of X-ray tomography

Eric Maire [a],[*], Paolo Colombo [b],[c], Jerome Adrien [a], Laurent Babout [d], Lisa Biasetto [b]

[a] *MATEIS Laboratory, UMR CNRS 5510, INSA de Lyon, France*
[b] *Dipart. di Ingegneria Meccanica, Settore Materiali, Università di Padova, Italy*
[c] *Manchester Materials Science Centre, University of Manchester, UK*
[d] *Department of Material Science and Engineering, The Pennsylvania State University, USA*

Abstract

X-ray tomography images of different cellular ceramics have been obtained using appropriate tomography setups. The samples exhibited a wide range of cell sizes (μm to mm) but a narrow range of porous fraction (75–85 vol.%). The images have been processed to retrieve the local fraction of ceramic. The average value of this measurement have been compared with a standard method based on image analysis of optical micrographs. The thickness distribution of both pores and ceramics was also retrieved using three-dimensional (3D) mathematical morphological operation on the images. The average value of these granulometry measurements was compared to optical and electron microscopy measurements.
© 2006 Elsevier Ltd. All rights reserved.

Keywords: Non-destructive evaluation; X-ray methods; Porosity; Microstructure-final; Porous-ceramics

1. Introduction

Many examples of cellular ceramics can be found in the natural world (see for instance the structure of shells or coral[1]), since their structure is very efficient from, among other properties, the strength/density ratio point of view. To exploit those favourable characteristics, several processing methods have recently been developed that allow the fabrication of components with a cellular structure made of metal, polymer or ceramic.[2] Among the different applications for highly porous ceramics, of great engineering relevance are filters for molten metal or particulate in a gas stream,[3] scaffolds for bone replacement or tissue culture,[4] porous burners,[5,6] kiln furniture[7] and components for many more specialized uses.[7] The main properties of interest for all these applications (permeability, thermal transport, strength, trapping efficiency, electrical conductivity) have a direct relation with the morphology of the cellular material.[8] The amount of porosity, the connectivity of the porous network, the size of the pores/cells, the dimension of the solid struts, the interconnections between cells are all key parameters for the optimisation of the cellular component to be employed for specific applications.[9] Thus, there is a crucial need for accurate methods to measure the above parameters constituting the cellular structure. The standard ways of imaging materials, based on the observation using appropriate microscopy techniques of the outer or fracture surface of these structures can provide straightforward solutions in some cases. Volume fraction can be derived from surface observations (besides being obtainable from density measurements). However, accurate image analysis does require some effort, and the investigation of a single or few cross-sections from a sample can fail to describe the material in its entirety (for instance in the case of a component with a graded porosity or a non isotropic morphology of the cell). The determination of the size of the various components (solid phase, pore/cell) is even more complex, as the exact shape of the pores or solid parts of the material are never completely well sampled by surface observations. This can be overcome in some cases thanks to stereology relations.[10] Nevertheless, when connectivity and tortuosity have to be precisely measured as in the case of providing data for modelling fluid transport within the porous component or acoustic absorption, one can only rely on the determination of the actual three-dimensional (3D) microstructure.

* Corresponding author. Tel.: +33 4 72 43 88 61; fax: +33 4 72 43 85 39.
E-mail address: eric.maire@insa-lyon.fr (E. Maire).

X-ray tomography is now a versatile technique which can quickly and simply provide 3D images of the actual microstructure[11,12] especially in the case of highly porous materials.[13–16] The images obtained by this technique can now be processed and analysed through 3D image analysis routines which have been recently developed and implemented.[17] The resolution of the technique has greatly improved thanks to the use of specialized equipments and is now of the order of 0.3 μm.[18] The aim of this paper is to present examples of quantitative analysis of the morphology of a wide range of different highly porous engineering components, which have been analysed by X-ray tomography, to illustrate the versatility of the technique as well as to compare the results with data obtained using conventional image analysis of optical micrographs.

2. Experimental conditions

2.1. Samples chosen

Six different cellular ceramic materials, possessing a similar, high level of porosity (∼75–85 vol.%) and an average cell size ranging from a few microns to a few millimetres were selected for this study. Conventional images of these samples (optical or scanning electron microscopy (SEM) micrographs, depending on the size of the microstruture) are shown in Fig. 1. Some of these materials were commercial products, such as a cordierite honeycomb (*Celcor®*, Corning Inc., Corning, NY, USA, sample labelled *Honey*) and two alumina foams of different cell size (*VUKOPOR®* A, Igor Láník - Techservis Boskovice, Boskovice, Czech Republic, samples labelled A_l and A_m). The other ceramic foam specimens were fabricated from a preceramic polymer (a methyl-silicone resin, MK, Wacker-Chemie GmbH, Munich, Germany) according to procedures previously reported[19,20] (samples labelled S_m, S_{50}, S_{10}). Apart from a different cell size, the samples possessed a varied morphology, in direct dependence on the fabrication method employed (see Fig. 1).[2] The honeycomb sample *Honey* possessed parallel channels with a square cross-section, because the raw materials were extruded through a die. The alumina foam samples were obtained by the replica technique (Schwartzwalder process), consisting in the dipping of a polymeric, open cell foam into a ceramic slurry, followed by sintering at high temperature. The resulting material is comprised by a web of ceramic rods (struts) encasing a continuously interconnected open porosity. Depending on the viscosity of the slurry and on the cell size of the starting polymeric foam, some cell walls (partially or completely obstructed interconnections between adjacent cells) can be found. The sample S_m was produced by a direct blowing technique (evaporation of a low boiling point solvent) and in the resulting morphology cell walls are well developed, and separate cells are connected through openings in the walls (cell windows). A strut in this material can be identified as the area where cells are in contact, forming a solid region with a triangular cross-section. Samples S_{50} and S_{10} were produced by the burn-out of sacrificial fillers (polymeric spherical microbeads), and the resulting morphology is very similar to that of a foam obtained by direct foaming techniques (see later—Fig. 6).

Standard relative density was determined by dividing the apparent density (measured by dividing the weight of the sample by its volume) by the true (or skeleton) density, obtained using a gas pycnometer (AccuPyc 1330, Micromeritics, Norcross, GA, SA) on finely ground powders. Image analysis (Image Tool 3.0, the University of Texas Health Science Center at San Antonio, San Antonio, TX, USA) was performed on images of the various samples obtained by digital photography, stereoscopic optical microscopy and scanning electron microscopy.

2.2. X-ray tomography image acquisition

The experimental part of this study focused on the use of a three-dimensional non destructive technique, the high resolution X-ray absorption tomography. Disturbance-free information about the microstructure throughout the volume could be obtained. Very detailed descriptions of this technique can be found in.[11,12] For the understanding of the present paper, the important features of this characterization method are briefly summarized here.

X-ray tomography is based on X-ray radiography, which allows the three-dimensional internal structure of a specimen to be determined non-destructively. When a X-ray beam passes through a sample, a radiograph can be formed, which is a projection of the absorption coefficients of the structures within the sample. Tomography involves rotating the sample about an axis perpendicular to the incident beam, and acquiring a series of radiographs at a sequence of angles. A filtered back-projection algorithm[21] can then be used to reconstruct the distribution of absorption coefficients within the volume of the sample. The result obtained after reconstruction is a regular array of the value of μ, the local attenuation coefficient of the X-rays measured for a cubic element of matter called a voxel (extension of the term pixel in 2D imaging). μ varies with the local composition and thus the internal structure of the sample can be determined without sectioning from this 3D regular map of μ. The resulting data can be analysed to obtain 3D information about the microstructure.

As the materials investigated had an average cell size spanning a wide range of values (from μm to mm), the resolution at which their morphology was mapped was different. The samples were thus scanned using two different tomographs:

- A standard laboratory tomograph located in the University of Manchester (UM); this apparatus is composed of a high power X-ray gun and two X-ray detectors everything being included in a self protected cabin; An X-ray fan beam with a source size of 9–10 μm is generated. Image magnification of the sample on the CCD detector, from 100 to 1.6 at the full scale (corresponding to pixel sizes of 1 μm up to 70 μm, respectively) are available depending on the source-sample distance. The radiographs have been acquired with a rotation path varying from 0.3 to 1° depending on the size of cellular structure and the sample (the larger size, the greater the rotation path).
- A high resolution X-ray tomograph located at the ESRF (beam line ID 19) in Grenoble (France).[18] In this case, paral-
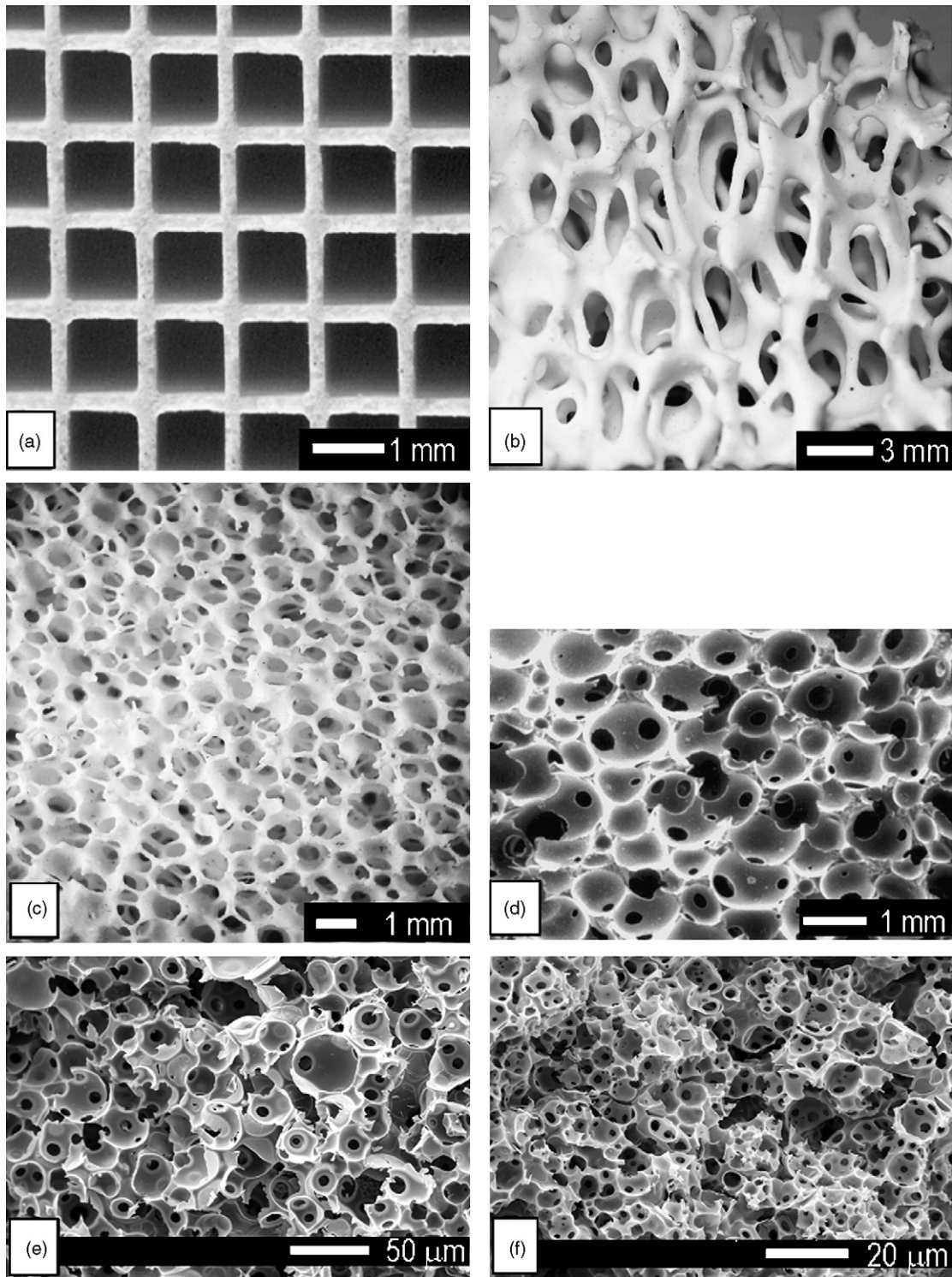
Fig. 1. General morphology of the samples used. Optical microscopy images of samples: (a) *Honey*; (b) A_l; (c) A_m. SEM micrographs of samples: (d) S_m; (e) S_{50}; (f) S_{10}.

lel beam X-ray tomography was performed at a resolution of 0.3 μm. The energy was set to 20 keV. The distance between the sample and the detector was about 5 cm fixing the amount of phase contrast to a minimum value (see [22] for more information on phase contrast). A set of 1800 projections were taken within 180°. The detector was a CCD camera with 2048 × 2048 sensitive elements coupled with an X-ray sen-

sitive laser screen. The field of view of the detector was about 0.6 mm wide.

2.3. Qualitative results

Fig. 2 a–f show qualitatively the images which have been obtained on the different selected materials. These include

bi-dimensional reconstructed grey level tomographic slices for each material. One can see from these images that the internal structure of the materials can clearly be imaged at various scales thanks to the strong difference in the attenuation coefficient between the solid and the gaseous phase. The figures also show in each case a three-dimensional rendering. These 3D images are obtained by drawing a surface between all the voxels exhibiting a same grey level. If this grey level is chosen as belonging to the limit between the solid and gaseous phase, the outer shape of the ceramic part can be rendered in 3D, the voxels belonging to the gaseous phase being transparent. Again, the structure are clearly visible in 3D. Note also that these rendering in Fig. 2 are quite similar to the conventional images obtained in Fig. 1.

Table 1 summarises the nature of the different materials and their anticipated cell size, the resolution (expressed as the voxel size in the reconstruction) and tomograph equipment used for scanning. It also identify each sample with a label. The samples presented all a random structure except the honeycomb (see Fig. 2).

3. Experimental results

3.1. Grey level image processing and thresholding

The 3D images obtained were processed and analysed. The last step of the process is the segmenstation which will separate
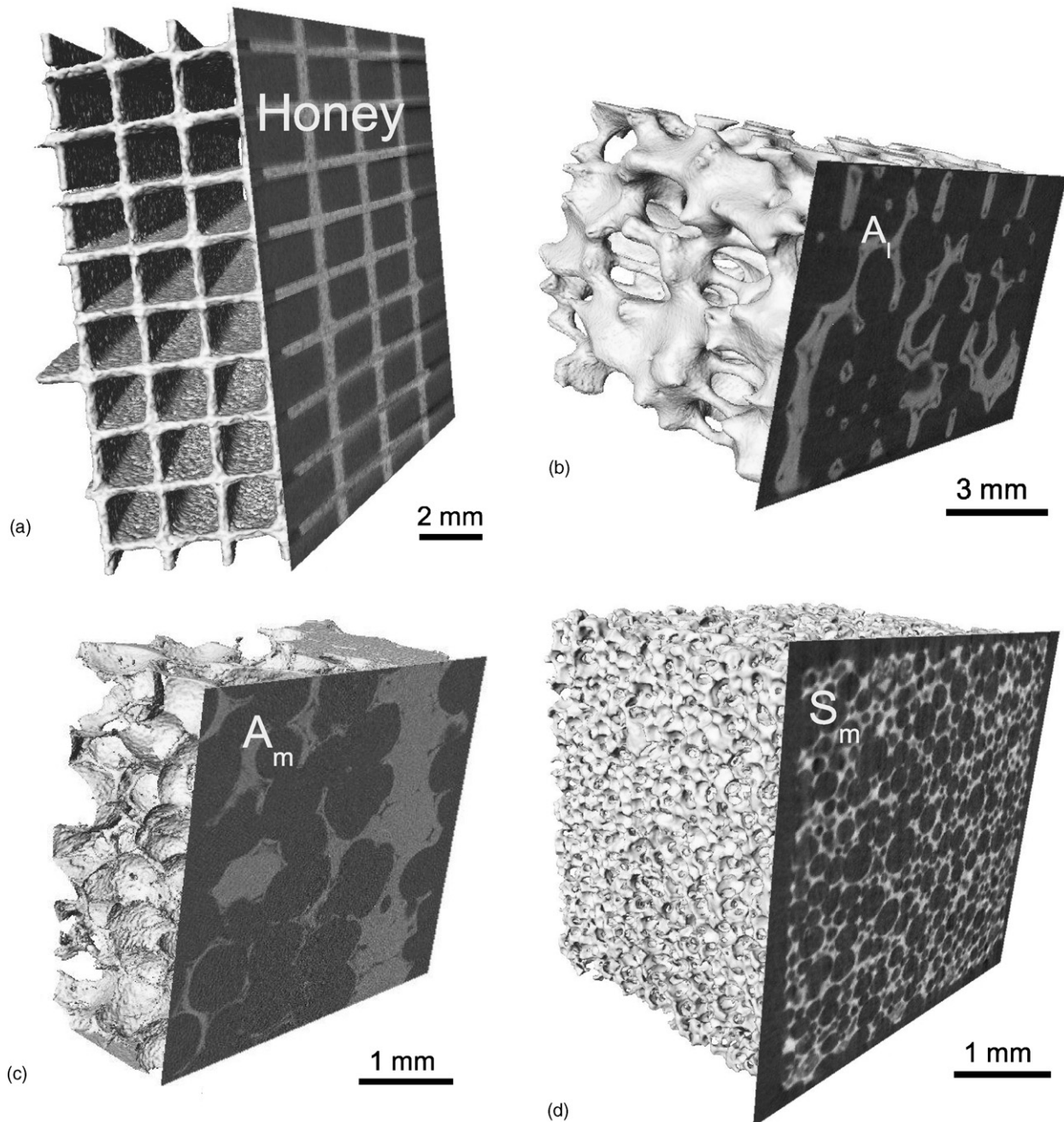

Fig. 2. 3D view and grey level tomographic slice for the six samples. (a) *Honey*; (b) A_l; (c) A_m; (d) S_m; (e) S_{50}; (f) S_{10}.
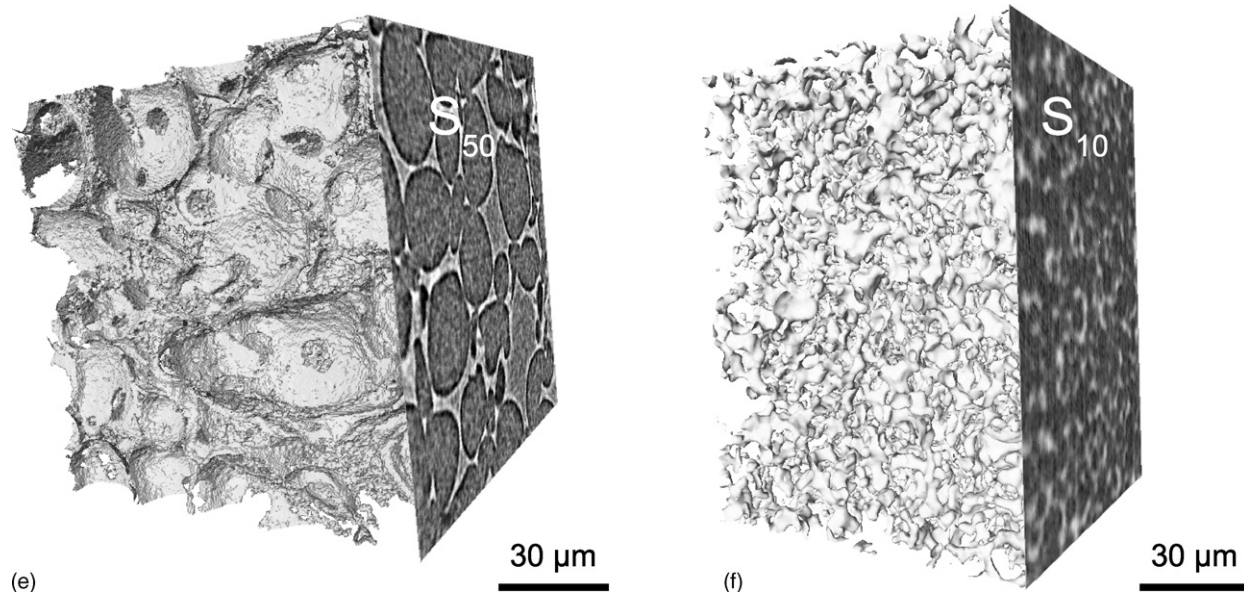
(e)   (f)

Fig. 2. (*Continued*).

all the voxels of the image into two families (black and white) which will hereafter be understood as belonging to the ceramic solid phase and the gaseous phase (contained in the empty cells), respectively. Naturally, the output of this processing step should resemble as closely as possible the actual microstructure of the specimens. The grey level images seem visually to be quite easy to separate into two families. However, depending on the quality of the initial images (i.e. the amount of noise included by the acquisition and reconstruction processes), the thresholding process was not always straightforward. In some cases, a series of images processing steps were applied to improve the grey level image and facilitate the last step. These steps included grey level equalisation and 3D median filtering over a neighbouring of one or two voxels depending on the amount of noise. In the case of the images obtained using the ESRF tomograph, the thresholding was even more tedious and was performed using a region growing procedure. Once thresholded, the images were analysed using the tools described in the following section.

3.2. Density measurement

The most simple characterisation of a porous material is to measure the density, by calculating the proportion of voxels belonging to the solid phase. This could be performed on a global manner in the six different studied samples counting the number of white voxels and dividing by the total size of the block in voxels. Because the tomographic data describes the three-dimensional structure, profiles of density calculated in slices as a function of position of each slice can be created. Fig. 3 shows, for two samples (*Honey* and A_l), typical profiles of the density values measured in each slice as a function of the slice number. This measurement was performed along two different directions (i.e. in two families of parallel slices) in each case. For statistical reasons, the average of the surface fraction over a sufficient number of this kind of slices is equal to the average fraction of porosity over the volume. Around this average, and at a different studied scale in each sample, the surface fraction in each slice in a given direction is quite strongly fluctuating. The profiles reported in Fig. 3 show this fluctuation. In sample *Honey*, it can be seen that the fraction in direction 1 is very homogeneous while it shows peaks of 100% of ceramic when the slice coincides exactly with a wall in direction 2. In sample A_l, the fraction is more homogeneous in direction 1 than in direction 2, where a higher concentration of ceramic is detected close to one of the faces of the sample. This higher ceramic content can be seen in the left side of the sample shown in Fig. 1b. The size of the studied blocks is not isotropic in the two cases and this explains why there are more measurements (because there are more slices) in

Table 1
Summary of the nature, the structure and the pore size of the samples studied

Ceramic material	Structure of the sample	Cell size	Tomograph used (μm)	Voxel size	Sample label
Cordierite	Honeycomb (oriented)	Large	UM	38	*Honey*
Al_2O_3	Foam (random)	Large	UM	80	A_l
Al_2O_3	Foam (random)	Medium	UM	20	A_m
SiOC	Foam (random)	Medium	UM	22	S_m
SiOC	Foam (random)	$\sim$50 μm	ESRF	0.3	S_{50}
SiOC	Foam (random)	$\sim$ 10 μm	ESRF	0.3	S_{10}

The tomograph equipment and the resolution used for the imaging are also listed in the table. The sample label will be used hereafter to identify the different specimens.
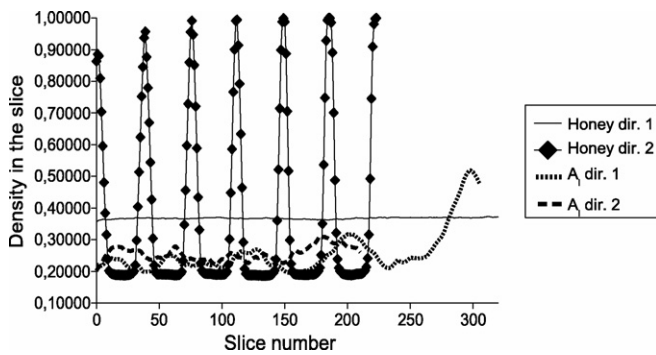
Fig. 3. Examples of volume fraction profiles of the ceramic as a function of the slice number in two samples (*Honey* and A_l samples) and in two directions for each material.

Fig. 4. Pore thickness distribution measurement performed on the six studied samples using mathematical morphology on the 3D images.

direction 1 than in direction 2. The fluctuation exemplified in the figure can be characterised by the variation coefficient equal to the standard deviation of the surface fraction over the slices divided by their average. The average density values and the variation coefficient (VC) have been obtained measuring along the three main perpendicular directions (*x*, *y* and *z*) for the different specimens, and are summarised in Table 2. The density values, obtained by conventional picnometry and weighing techniques are also reported in the last column (relative density standard).

3.3. Size distribution

In addition to the simple measurement of the density, it is useful to obtain a measure of the characteristic size of each of the two phases (the pores—cell size—and the ceramic matrix—comprising both the strut size and the cell wall thickness). Measuring a typical size of an interconnecting network of two phases is not a trivial procedure. Standard image processing measures size by agglomerating connected voxels and measuring the dimensions of each aggregate, but this only works if the objects to be measured are isolated in a matrix. In the case of co-continuous (interpenetrating) networks of two phases—as for the samples we analysed in this work—a typical size can be calculated using a computational processing procedure composed of a sequence of standard mathematical morphology operations applied to the binarised 3D images. This sequence of operation allows to measure the granulometry (i.e. the density distribution of the thickness) of the studied phase in the material. Sequential 3D morphological erosion and dilation operations of increasing size are applied to the phase of interest. After an erosion operation of thickness *t*, all features with a characteristic thickness
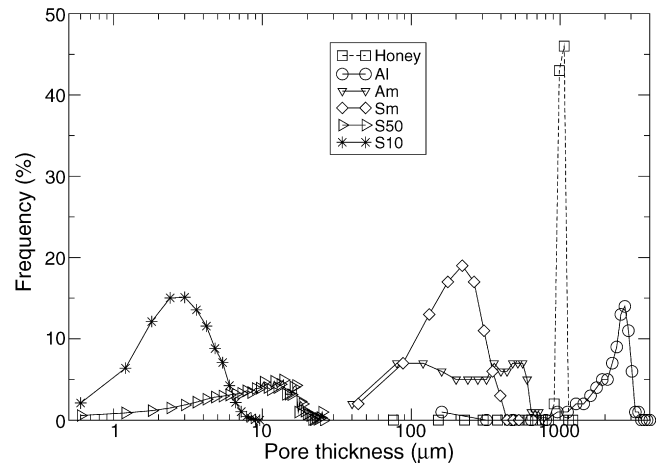
smaller than 2*t* will disappear. A subsequent dilation operation of thickness *t* starting from the eroded structure will restore only those features with a characteristic thickness greater than 2*t*. By counting the number of voxels remaining after each erosion and dilation, as a function of *t*, a histogram can be obtained describing what proportion of the phase is contained in features of which size. This operation can be applied to both phases of the binary image, to describe the pores (empty cells) and the ceramic matrix. More details on this method can be found in.[17] Figs. 4 and 5 compare, for the six samples investigated, the thickness histograms measured on the gaseous phase (porosity) and the ceramic phase, respectively. Given the large distribution of typical sizes covered in the present study, the scale of the thickness horizontal axis of the figure is logarithmic. These histograms can be processed to retrieve the value of the average and of the standard deviation (allowing to calculate the variation coefficient of the distributions) of the measured thickness distributions. A summary of these quantifications is given in Table 3.

In order to compare these results with ones derived from classical analytical procedures, image analysis was performed on micrographs of the various samples obtained using different imaging techniques. A couple of images were analysed per each specimen, and at least 50 measurements were obtained per each feature considered. A stereological correction factor was applied to determine the true three-dimensional mean cell size (D_{sphere}), considering that the average circular segment diameter (D_{circ}, as determined directly by image analysis) is smaller due to random

Table 2

Summary of the density values obtained from processing of tomography data along three perpendicular directions for each studied sample

Material	Relative density tomo (%)	VC_x (%)	VC_y (%)	VC_z (%)	Relative density standard (%)
Honey	36.8	0.75	75	80	21.2
A_l	25.6	8.9	27	19	14.9
A_m	36.6	9	53	37	15.2
S_m	33.4	4.4	12	7	24.3
S_{50}	23.8	9	16	11	15.8
S_{10}	21	6	4	5	14.6

The average value is the same in each case, but the variation coefficients (VC) are different. The data obtained using conventional techniques is also reported in the last column.
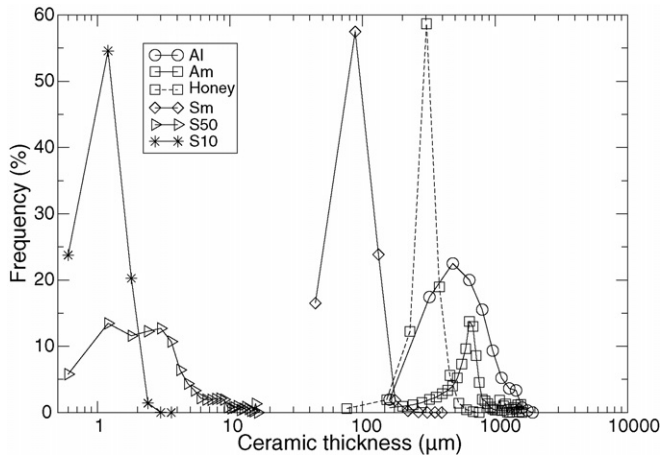
Fig. 5. Ceramic thickness distribution measurement performed on the six studied samples using mathematical morphology on the 3D images

truncation of the cells with respect to the depth at the plane of the specimen surface. According to,[23] the relation can be expressed by the equation: $D_{sphere} = D_{circ}/0.785$. In Fig. 6 are shown two micrographs detailing the various features (cell size, cell window size, strut size) that were quantified by image analysis in the ceramic foams. The result of these standard measurements is given in Table 4.

4. Discussion

Density measurements shown in Table 2 indicate that the values obtained using image processing of X-ray tomography tend to be higher than the measurements performed using standard weighing methods. This is probably partly due to an effect linked with the high specific surface in the materials under study and to the limited resolution of the technique used to obtain the images. In the case of cellular materials with high specific surface, the amount of solid located in thin regions is quite important. In these thin regions, a mis-approximation of one voxel on each
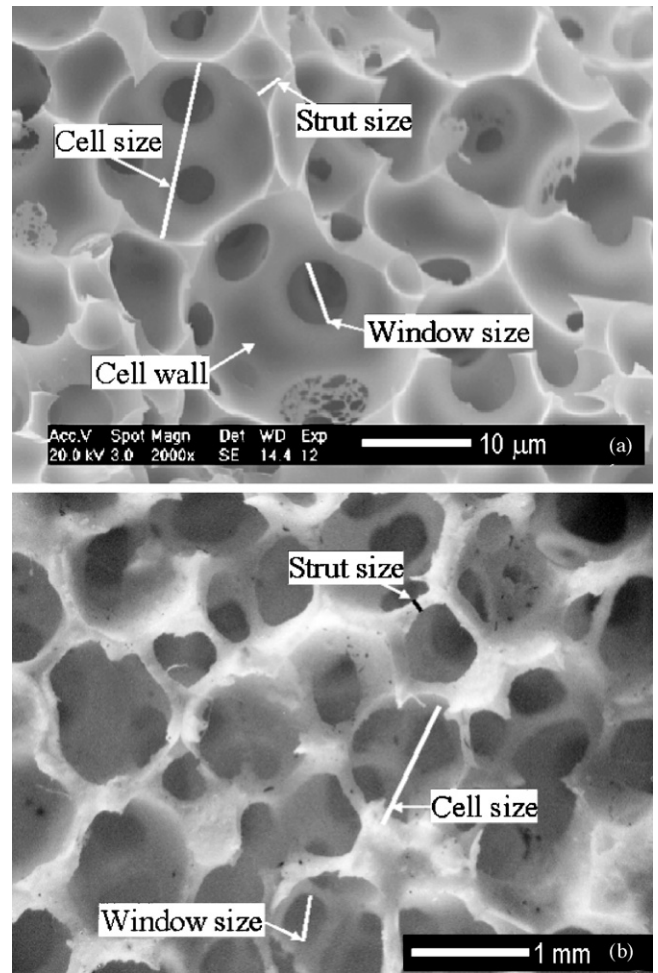

Fig. 6. Identification on optical micrographs of the dimensional characteristics (pore-cell size, ceramic thickness – strut size –, cell window size), that can be quantified using images analysis. (a) Sample S_{10}; (b) sample A_m.

Table 3
Summary of the thickness distribution measurements performed using the mathematical morphology method for each studied sample

Material	Average thickness tomo pores (μm)	VC (%)	Average thickness tomo ceramic (μm)	VC (%)
Honey	998	1	318	3
A_l	2380	17	680	38
A_m	351	50	647	29
S_m	220	21	93	7
S_{50}	11.6	35	3.8	93
S_{10}	3.4	34	1.2	17

The average is given in μm for both pores and ceramic together with the variation coefficients of each distribution.

Table 4
Summary of the size measurements (cell size, strut size, cell window size see Fig. 6) for each sample, performed on optical images

Sample	Pore size (μm)	VC (%)	Ceramic strut size (μm)	VC (%)	Cell window (μm)	VC (%)
Honey	985	4	317	4	–	–
A_l	3610	12	510	13	2160	25
A_m	1060	36	134	27	686	27
S_m	1100	16.4	212	23	261	34
S_{50}	29.3	21	5	20	6.4	22
S_{10}	7.9	26	1.1	27	1.5	33

The average cell window size is also reported for completeness.

side of the thickness leads immediately to a quite strong variation of the fraction of solid phase measured. In most of the cases when the structures are thin, the thresholding tend to be a bit conservative i.e. threshold is fixed at a value chosen to make sure that the cells are closed in the binarized image. This was for example observed in the thresholding of thin shells of hollow glass spheres in syntactic foams.[24] The density of the solid phase is probably a bit overestimated because of this combination of low thickness of the solid phase and over thresholding. In the case of sample A_m, we verified that if the threshold value is strongly changed, the volume fraction of ceramic can for instance be reduced from 25.6% down to about 20.7%. This brings the measured value closer to the 14.9% measured using the standard method. In this respect, it would always be better to increase slightly the resolution in the images but this would also increase the size and the processing time of a given image. We believe however that the resolution chosen in each studied case is sufficiently small compared to the size of the cellular structure to be studied. The observed difference is probably rather due to the presence of very fine pores, undetected by the X-ray tomography technique and thus considered as ceramic phase. In fact, most cellular ceramic components are not sintered to full density, in order to reduce shrinkage and cost.[2,7] It should be noted that the presence of hollow struts—typical of reticulated ceramics—can be accounted for in the tomographic analysis (see for instance the bi-dimensional reconstructed slice for sample A_l in Fig. 2 where the hollow struts can clearly be seen). In the case of the samples S_{10} and S_{50} analysed using synchrotron images, there is also probably an effect of the perturbation of the thresholding process by the presence of phase contrast fringes[25] which modifies the contrast especially when the structure is thin. It can also be seen in Fig. 2f that the resolution is just about sufficient to image clearly the structure of the S_{10} sample. For all these reasons the absolute value measured using X-ray tomography should be considered with due care. The relative values of these measurements can however be compared and with this restriction, the superiority of the measurement made by tomography is that it allows the homogeneity of the ceramic fraction to be quantitatively measured in different locations of the sample, as shown by the profiles in Fig. 3. Moreover, the volumetric morphological data can serve as input for studies predicting important characteristics of a cellular ceramic component, such as permeability, mechanical or thermal properties.

The comparison of the size measurements performed using both tomographic images and SEM images also calls for some comments. Except for the *Honey* sample, for which the measurements coincide nicely, the thickness measurements performed using 3D granulometry of tomographic images tend to give smaller size measurement than the SEM images. In the case of a percolating phase like the ones we have in the 3D images (both the solid and the gaseous phases are percolating in each material except in the *Honey* sample), it is difficult to measure a size properly, because the typical size of the cluster of voxels forming the phases is equal to the size of the studied block. Therefore, mathematical morphology has been here employed for the data analysis. As mentioned before, this method is based on a set of opening operations of the 3D images, the size of the

structural element increasing for each successive opening operation. This, then only allows to measure the amount of material (solid or gaseous phase) exhibiting a given thickness, the typical result of which is plotted in Figs. 4 and 5. The thickness measured corresponds to the smallest dimension of the given phase. It is thus natural for this value to be smaller than the one obtained by using image analysis of optical micrographs, as shown in Fig. 6 because in this latter case we do not measure the smallest dimension but rather the average size of the cell. The average thickness measured in some cases can be two times (cell size of samples S_{10} and S_{50}) or even three times (cell size of sample A_m) smaller in the case of tomography than for standard image analysis. This is also due to the fact that, when performing image analysis using optical micrographs, we measured the equivalent diameters of the cells present in the material, assuming them to be spherical; however, the porosity (cell) has in reality a much more complex shape. Tomography analysis, instead, is capable of sampling the full, actual morphology of a sample; this tends, in average, to lower the typical thickness of the features considered. Moreover, considering the "thickness" of the ceramic phase, image analysis can easily give the strut dimension, but its use is much less straightforward for determining the cell wall thickness. Instead, the data obtained using tomography, comprise at the same time both the "strut size" and the "cell wall size", without distinguishing between the two morphological characteristics of the solid ceramic phase. This distinction can in some cases be highlighted by the presence of two peaks in the distribution as observed when characterising metal foams in [17] but it does not seem to be obvious in the present case (see Fig. 5). In summary, none of the measurements obtained using the two different techniques are to be considered wrong, but the values shouldn't be compared directly—especially in the case of porous (cellular) specimens—as they are intrinsically related to characteristics of the materials' morphology which are not completely equivalent.

In general, 3D images are meant to be more appropriate for morphology quantification than 2D ones especially for the measurement of feature size and feature number in the case of complex shape as it is obviously the situation in this work. However, the quantification of one of the microstructural parameters, i.e. the size of the windows connecting the pores, is particularly easier to perform using image analysis of micrographs than using tomography. This is because optical and electronic microscopy can image with no blur the structure over a large depth, and also because, when dealing with porous materials, one of the phases is transparent to the light or to the electrons. In these two conditions, it becomes very easy to measure precisely and with limited bias the size of the interconnecting windows between each cells in samples where these windows exist (see Table 4). The measurement of these interconnecting windows can be of particular value for the characterisation of transfer properties within cellular structures. It is in principle possible to measure these features from the 3D images performing successive mathematical morphology operations but this difficult image processing implementation was out of the scope of the present study.

Finally, it is worth noting that the values obtained coincide when analysing a sample like *Honey* with a more homogeneous

morphology (regularly shaped cells and uniform cell wall size), using different experimental techniques. In agreement with the above discussion, in fact, in this case there is no difference in the morphological features measured by tomography and image analysis. Also, due to the regularity of the structure, a very low variation coefficient is found.

5. Conclusions

X-ray tomography images of different cellular ceramics were collected using appropriate equipment setups. The samples were chosen to exhibit a wide range of size (μm to mm) but a narrow range of porosity (75–85 vol.%). The images were processed to retrieve the spatial distribution of the local fraction of ceramic (measured in slices). The average density values obtained by tomography have been compared with those from a conventional (gravimetric) method. It has been shown that the two measurements disagree, probably because 3D image processing of the tomography images overestimates the density. The reason for this is that the part of the samples recognised as 'solid' by the tomography technique actually contains very fine pores, the ceramic being not fully sintered. At the resolution used to analysed the cell size, these tiny pores can not be distinguished. The thickness distribution of both the pores (cells) and the solid (ceramic) phase was also retrieved using 3D mathematical morphological operations on the tomographic images. The average value of these granulometry measurements was compared to the data obtained from image analysis of optical micrographs. This was found to be smaller in all cases, except when the architecture of the sample is very uniform, as in the case of a honeycomb. This can be explained by the fact that, particularly in the case of porous (cellular) solids, the tomographic 3D image processing method measures different morphological features from those quantified using image analysis of optical micrographs. It can then be concluded that standard measurements and those obtained using new 3D methods should be compared with caution. The combination of these two types of measurement give a very complete and complementary picture of the microstructure and morphology of porous ceramics which is likely to enrich the description of these materials.

Acknowledgements

References

1. Perkowitz, S. *Universal Foam: From Cappuccino to the Cosmos*. Walker and Company, 2000.
2. Colombo, P., Conventional and novel processing methods for cellular ceramics. *Philos. Trans. R. Soc. A* 2006, **A364**, 109–124.
3. Gauckler, M. M. W., Conti, C. and Jacob-Duliere, M., Industrial application of open pore ceramic foam for molten metal filtration. *Light Metals* 1985, 1261–1283.
4. Rodrguez-Lorenzo, L. M. and Ferreira, J. M. F., Development of porous ceramic bodies for applications in tissue engineering and drug delivery systems. *Mater. Res. Bull.* 2004, **39**(1), 83–91.
5. Pickencker, O., Pickencker, K., Wawrzinek, K., Trimis, D., Pritzkow, W. E. C., Mller, C., *et al.*, Innovative ceramic materials for porous medium burners i. *Interceram* 1999, **48**, 326–330.
6. Pickencker, O., Pickencker, K., Wawrzinek, K., Trimis, D., Pritzkow, W. E. C., Mller, C., *et al.*, Innovative ceramic materials for porous medium burners ii. *Interceram* 1999, **48**, 424–434.
7. M. Scheffler, P. Colombo P, ed. In *Cellular Ceramics: Structure, Manufacturing Properties and Applications*. Wiley-VCH Verlag GmbH, Weinheim, Germany, 2005.
8. Gibson L. J. and Ashby M. F. In *Cellular Solids, Structure and Properties* (*2nd ed.*). Cambridge University Press, Cambridge, England, 1999.
9. Green, J. and Colombo, P., Cellular ceramics: Intriguing structures, novel properties, and innovative applications. *MRS Bull.* 2003, **28**(4), 296–300.
10. DeHoff, T. and Rhines, F. N., *Quantitative Microscopy*. Mc Graw-Hill Book Company, 1968.
11. Maire, E., Buffière, J. Y., Salvo, L., Blandin, J. J., Ludwig, W. and Letang, J. M., On the application of X-ray microtomography in the field of materials science. *Adv. Eng. Mater.* 2001, **3**(8), 539–546.
12. Buffière, J. Y., Maire, E., Cloetens, P., Lormand, G. and Fougères, R., Characterization of internal damage in a MMCp using X-ray synchrotron phase contrast microtomography. *Acta Mater.* 1999, **47**(5), 1613–1625.
13. Maire, E., Elmoutaouakkil, A., Fazekas, A. and Salvo, L., In situ measurements of deformation and failure of metallic foams using X-ray tomography. *MRS Bull.* 2003, **28**, 284.
14. Maire, E., Fazekas, A., Salvo, L., Dendievel, R., Youssefand, S., Cloetens, P., *et al.*, X-ray tomography applied to the characterization of cellular materials. Related finite element modeling problems. *Compos. Sci. Technol.* 2003;**63**:2431–2443.
15. Bart-Smith, H., Bastawros, A. -F., Mumm, D. R., Evans, A. G., Sypeck, D. J. and Wadley, H. N. G. *Acta Mater.* 1998, **46**, 3583–3592.
16. Babout, L., Mummery, P. M., Marrow, T. J., Tzelepi, A. and Withers, P. J., The effect of thermal oxidation on polycrystalline graphite studied by X-ray tomography. *Carbon* 2005, **43**, 765–774.
17. Elmoutaouakkail, A., Salvo, L., Maire, E. and Peix, G., 2d and 3d characterisation of metal foams using X-ray tomography. *Adv. Eng. Mater.* 2002, **4**(10), 803–807.
18. Boller, E., http://www.esrf.fr.
19. Colombo, P. and Hellmann, J. R., Ceramic foams from preceramic polymers. *Mat. Res. Innovat.* 2002, **6**, 260–272.
20. Colombo, P., Bernardo, E. and Biasetto, L., Novel microcellular ceramics from a silicone resin. *J. Am. Ceram. Soc.* 2004, **87**(1), 152–154.
21. Feldkamp, L. A., Davis, L. C. and Kress, J. W., Practical cone beam algorithm. *J. Opt. Soc.* 1984, **1**(6), 612.
22. Cloetens, P., Pateyron-Salome, M. and Buffière, J. Y., Observation of microstructure and damage in materials by phase sensitive radiography and tomography. *J. Appl. Phys.* 1997, **81**(9), 5878–5886.
23. ASTM Standards, Standard test method for cell size of rigid cellular plastics. *ASTM, D* 1977, **3576**, 919–922.
24. Maire, E., Gimenez, N., Sauvant-Moynot, V. and Sauterau, H., X-ray tomography and three-dimensional image analysis of epoxy-glass syntactic foams. *Philos. Trans. R. Soc.* 2006, **364**, 69–88.
25. Cloetens, P., Pateyron-Salome, M., Buffiere, J. -Y., Peix, G., Baruchel, J., Peyrin, F., *et al.*, *J. Appl. Phys.* 1997, **81**, 9.